ASL TR-0303

A METHOD FOR ESTIMATING SIMILARITY SCALING AND OBUKHOV LENGTHS FROM DISCRETE VERTICAL PROFILE DATA

December 1991

Henry Rachele
Arnold Tunick
Frank V. Hansen

US ARMY
LABORATORY COMMAND
ATMOSPHERIC SCIENCES LABORATORY
White Sands Missile Range, NM 88002-5501

NOTICES

Disclaimers

The findings in this report are not to be construed as an official Department of the Army position, unless so designated by other authorized documents.

The citation of trade names and names of manufacturers in this report is not to be construed as official Government indorsement or approval of commercial products or services referenced herein.

Destruction Notice

When this document is no longer needed, destroy it by any method that will prevent disclosure of its contents or reconstruction of the document.

REPORT DOCUMENTATION PAGE

Form Approved
OMB No. 0704-0188

1 AGENCY USE ONLY (Leave blank)	2 REPORT DATE	3 REPORT TYPE AND DATES COVERED
	December 1991	Final

4 TITLE AND SUBTITLE

A Method for Estimating Similarity Scaling and Obukhov Lengths from Discrete Vertical Profile Data

5 FUNDING NUMBERS

6 AUTHOR(S)

Henry Rachele, Arnold Tunick, and Frank V. Hansen

5 FUNDING NUMBERS

B53A-B 6II102.53A40.11

7 PERFORMING ORGANIZATION NAME(S) AND ADDRESS(ES)

U.S. Army Atmospheric Sciences Laboratory
White Sands Missile Range, NM 88002-5501

8 PERFORMING ORGANIZATION REPORT NUMBER

ASL-TR-0303

9 SPONSORING MONITORING AGENCY NAME(S) AND ADDRESS(ES)

U.S. Army Laboratory Command
Adelphi, MD 20783-1145

10 SPONSORING MONITORING AGENCY REPORT NUMBER

11. SUPPLEMENTARY NOTES

12a. DISTRIBUTION AVAILABILITY STATEMENT

Approved for public release; distribution is unlimited.

12b DISTRIBUTION CODE

13. ABSTRACT *(Maximum 200 words)*

Many schemes have been developed to transform discrete meteorological vertical profile data into continuous forms. However, problems with fitting highly nonlinear equations such as similarity formulations to discrete values of wind, temperature, and specific humidity in the surface boundary layer still exist, since the data deviates from the smooth theoretical profiles due to natural fluctuations and instrument errors. The authors have compared the results of the tried-and-true method with the results of their method that is based on the mean value theorem of calculus. The authors have dealt with the unstable, stable, and neutral cases, showing no significant difference in using either method.

14. SUBJECT TERMS

micrometeorology, surface boundary layer, similarity scaling parameters, Obukhov scaling length, windspeed, temperature, specific humidity, mean value theorem

15. NUMBER OF PAGES

30

16. PRICE CODE

17. SECURITY CLASSIFICATION OF REPORT	18. SECURITY CLASSIFICATION OF THIS PAGE	19. SECURITY CLASSIFICATION OF ABSTRACT	20. LIMITATION OF ABSTRACT
Unclassified	Unclassified	Unclassified	SAR

CONTENTS

LIST OF ILLUSTRATIONS 4

1. INTRODUCTION 5

2. PROFILE SMOOTHING TECHNIQUES 5

3. RACHELE/TUNICK (RT) APPROACH 10

4. CALCULATION PROCEDURES 15

5. RESULTS 16

6. CONCLUSIONS 19

LITERATURE CITED 21

APPENDIX A. RACHELE/TUNICK (RT) APPROACH 23

APPENDIX B. THEOREM OF THE MEAN 27

DISTRIBUTION LIST 29

LIST OF ILLUSTRATIONS

Tables

1. The Universal Geometric Progression for Micrometeorological Measurements with a = 1, r = 2 7

2. Similarity Constants and Computed Reference Heights 17

Figures

1. Fitted profiles to temporally meaned experimental data at observational heights 6

2. Normalized wind and temperature profiles illustrating advection of heat above 1 m in the surface boundary layer 9

3. Illustrative wind profile as formulated in equation (15) 12

4. Windspeed profile in the surface boundary layer for the neutral case 17

5. Windspeed profiles in the surface boundary layer for the unstable case 18

6. Temperature profiles in the surface boundary layer for the unstable case 18

B-1. Illustration of the mean value theorem for a given function f(x) .. 27

1. INTRODUCTION

Many schemes have been developed to transform discrete meteorological vertical profile data into continuous forms. The roots of profile analysis apparently are buried in the past; a comprehensive literature search failed to produce any documentation pertaining to the origins or a postulate to serve as a basis for data analysis. Although these "a priori" techniques work well, problems with fitting highly nonlinear equations such as similarity formulations to discrete values of wind, temperature, and specific humidity in the surface boundary layer exist, since the data deviates from the smooth theoretical profiles due to natural fluctuations and instrument errors. As a first step, since the data are discrete, micrometeorologists have suggested that the measuring devices be spaced exponentially (for instance, 1/4, 1/2, 1, 2, 4, and 8 m above the surface). A second approach is to plot the data at the heights where they were measured, and fit a smooth curve by eye through these data points, and then pick off values at the geometric mean heights. These data are then used to calculate values of the unknown constants and variables inherent in the profile formulations. Of the methods available, we have selected a technique used by one of the authors based upon information from Panofsky (1963) and Businger et al. (1971) (which has worked rather successfully) illustrating the tried-and-true approach. Then we present a method we have developed that is based on the mean value theorem of calculus.

2. PROFILE SMOOTHING TECHNIQUES

Hypotheses concerned with the structure of turbulence in the surface boundary layer of the atmosphere generally follow the central limit theorem--the fundamental frequency distribution of statistical analysis. This would intuitively imply that the mean flow is stationary and homogeneous. In actuality, over short-time intervals, the atmosphere may be assumed stationary, but not homogeneous. Ellison's (1957) infinite rough plane does not exist as a real surface. The surface of the earth consists of roughness elements that vary with height and, at best, are randomly distributed. These protuberances, when coupled with vertical sensible heat fluxes, have a profound effect upon the mean flow. The mechanical and convective production of turbulence generates a state of fluid flow where the instantaneous eddy velocities exhibit apparently random fluctuations. Thus, in practice only statistical properties can be recognized and ultimately analysed.

Micrometeorological data collected on a tower or mast over some finite sampling time must be smoothed as a preanalysis operation. Means and standard deviations for each measured entity are formed at each measurement height above the surface. Plotting the temporally averaged data as a function of height and smoothing by eye, as illustrated in figure 1, reveal that the averaged data exhibit a root-mean-square error (rmse) distribution about the simulated vertical profile curves. The rmse can be attributed to variable upwind fetches, a random distribution of roughness elements, a nonuniform vertical flux of sensible heat, and induced vertical motions.

This arbitrary empirical smoothing technique can be improved by considering that the vertical profiles in the surface boundary layer are measured in an environment where the data are limited at one end of the range and unlimited at the other. Also, the data tend to show a constant rate of change from one

height value to the next. These are the characteristics of values that form a geometric progression, that is, follow the exponential law

$$z = a\, r^{b} \quad , \tag{1}$$

where z is height above the surface, a and r are constants, and b is variable. Equation (1) is usually referred to as the law of natural growth. For micrometeorological data, international agreement requires that measurements be made at heights based upon the progression listed in table 1.

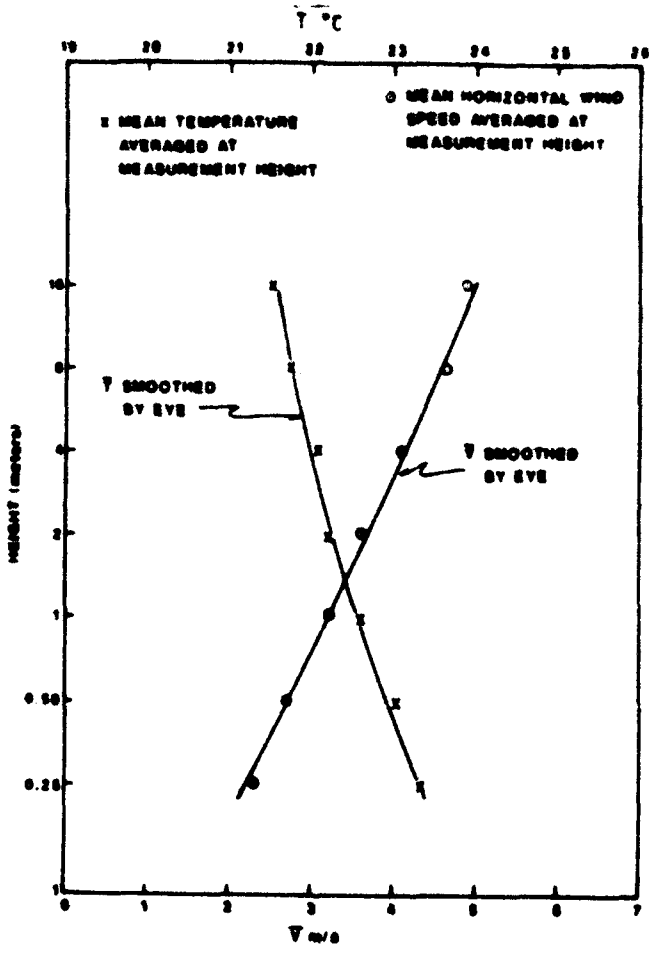

Figure 1. Fitted profiles to temporally meaned experimental data at observational heights.

TABLE 1. THE UNIVERSAL GEOMETRIC PROGRESSION FOR MICROMETEOROLOGICAL MEASUREMENTS WITH a = 1, r = 2

b	-2	-1	0	1	2	3	4	5	6 . . .
z (m)	0.25	0.5	1	2	4	8	16	32	64 . . .

Using such a scheme for observing profile data ultimately simplifies the analysis, owing to the fact that the implied vertical gradients through a layer from z_1 to z_2 are always tangent to the profile at the geometric mean height $z_g = (z_1 z_2)^{1/2}$.

Businger et al. (1971) found that in thermally stratified unstable flow conditions, a differentiated second-order polynomial in ln(z) provided an excellent fit to the raw data. For a stable regime the polynomial cz = a + bln(z) was used. This procedure provides a more exacting fit than the semi-empirical technique of figure 1.

At this point, a preliminary analysis of the data must be undertaken. The profiles must be smoothed in the vertical to assure equilibrium with the local roughness and heat flux environment. Gradient Richardson (1920) numbers are calculated for each geometric mean height. Sutton (1953) indicates that the gradient Richardson number is given by

$$Ri = \frac{g}{\bar{\theta}} \frac{\partial\bar{\theta}/\partial z}{(\partial V/\partial z)^2} \quad , \tag{2}$$

where g is the gravitational acceleration, $\bar{\theta}$ the potential temperature, and $\bar{V}$ the mean horizontal windspeed. The overbar represents a temporal average. Equation (2) may be restated in a more useful form as

$$Ri = \frac{g}{\bar{\theta}} \frac{(\Delta\theta + \Delta z\Gamma)}{(\Delta V)^2} z_g \Delta\ln z \quad , \tag{3}$$

where Γ is the dry adiabatic lapse rate.

Using an approximation for the height derivative of Ri for an unstable atmosphere, as implied by Lettau (1957),

$$L^{-1} = \frac{\Sigma(Ri)z}{\Sigma(z)_i} \quad ; \quad i = 1, 2, 3, \ldots \quad , \tag{4}$$

a value of the Obukhov (1946) scaling length L is obtained for the observed profile conditions for unstable flow, if the premise that the Monin and Obukhov (1954) scaling ratio z/L is equal to Ri is accepted.

It follows then that the surface friction velocity, u*, takes the form

$$u^* = \frac{k(V_2 - V_1)}{\phi_m \ln\left[\frac{z_2}{z_1}\right]} \quad \text{where } \phi_m = \left(1 - 15\,\frac{z}{L}\right)^{-1/4} , \tag{5}$$

and that the temperature scaling parameter, T*, can be calculated by

$$T^* = \frac{k(\theta_2 - \theta_1)}{\phi_H \ln\left[\frac{z_2}{z_1}\right]} \quad \text{where } \phi_H = \left(1 - 15\,\frac{z}{L}\right)^{-1/2} . \tag{6}$$

In a stable regime this is not the case. Investigations by Webb (1970), Oke (1970), and Hicks (1976) suggest that in stable flow the profiles are log-linear. Hansen (1977) found that

$$\frac{z}{L} = Ri\ \phi_m \tag{7}$$

and

$$\phi_m = (1 + 15\ Ri) . \tag{8}$$

Again, values of Ri at each geometric mean height are calculated and the Monin-Obukhov scaling ratio determined from

$$\frac{z}{L} = Ri(1 + 15\ Ri) . \tag{9}$$

The representative values of z/L for such z_g are then calculated by using equation (9) and the Obukhov length from

$$L^{-1} = \frac{\Sigma(z/L)z}{\Sigma(z_i)} . \tag{10}$$

If the Obukhov length L or the scaling ratio z/L are readily available and the gradient Richardson numbers are desired, then

$$Ri = -0.0333 \left[1 - (1 + 60)\frac{z}{L}\right]^{1/2} , \qquad (11)$$

as suggested by Sutherland, Hansen, and Bach (1986).

Roughness and albedo discontinuities in the upwind direction will appear in the analysis through a relationship with horizontal advection. These heterogeneous effects may be detected using an approach suggested by Panofsky (1963). If $\ln z + \psi (z/L)$ is plotted as a function of $\bar{V}$, $\bar{\theta}$, then k/u^* or k/T^* will be the profile slope and $\ln z_o$ or T_o the intercept.

Advection effects upon profiles are illustrated in figure 2. The plotted wind data lie upon the theoretical profile while the temperatures in the upper portion diverge towards warmer values indicating horizontal advection of heat. If advective effects are not recognized early on in the analyses of profile data, erroneous conclusions are easily formed, and the values of the diabatic constants and variables more easily misinterpreted.

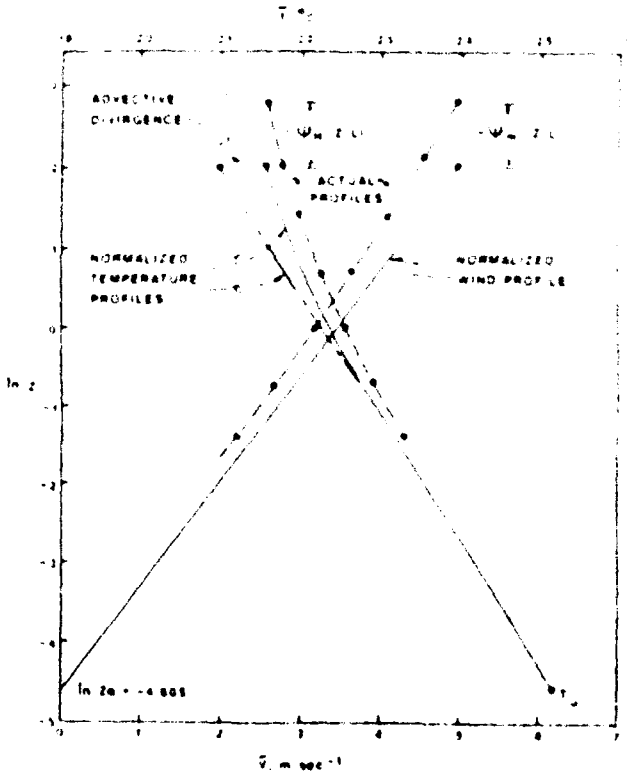

Figure 2. Normalized wind and temperature profiles illustrating advection of heat above 1 m in the surface boundary layer.

We surmise that the geometric progression approach for establishing vertical gradients had its origins in the mean value theorem of calculus. This inference will be explored in section 3.

3. RACHELE/TUNICK (RT) APPROACH

Based upon the Obukhov (1946) theory and the mean value theorem, this approach first assumes that the wind, potential temperature, and specific humidity vertical profiles are representable by damp similarity forms, the gradients of which are given below for unstable conditions.*

$$\frac{\partial \bar{V}}{\partial z} = \frac{u^*}{kz}\left(1 - \beta \frac{z}{L}\right)^{-1/4} \tag{12}$$

$$\frac{\partial \bar{\theta}}{\partial z} = \frac{\theta^*}{kz}\left(1 - \gamma \frac{z}{L}\right)^{-1/2} \tag{13}$$

$$\frac{\partial \bar{q}}{\partial z} = \frac{q^*}{kz}\left(1 - \gamma \frac{z}{L_v}\right)^{-1/2}, \tag{14}$$

where

V = windspeed

z = height

u^* = friction velocity

k = Karman's constant

L = Obukhov length = $-u^{*2}T_r/kg\theta^*$

θ = potential temperature of moist air

θ^* = potential temperature scaling length

g = acceleration due to gravity

T_r = reference level temperature

L_v = moisture modified Obukhov length = $-u^{*2}T_{vr}/kg\theta_v^*$

*The neutral and stable cases are treated in appendix A.

T_{vr} = virtual temperature = $T_r(1 + 0.61\ q_r)$

$\theta_v^* = \theta^* + 0.61\ \theta\ q^*$

Integrating equations (12) through (14) yields

$$V(z) = V(z') + \frac{u^*}{k}\left\{\ln\left(\frac{x-1}{x+1}\right) + 2\tan^{-1}x\right\}\Bigg|_{x'}^{x} \tag{15}$$

$$\theta(z) = \theta(z') + \frac{\theta^*}{k}\left\{\ln\left(\frac{y}{y+1}\right)\Bigg|_{y'}^{y}\right\} \tag{16}$$

$$q(z) = q(z') + \frac{q^*}{k}\left\{\ln\left(\frac{y_L}{y_L+1}\right)\Bigg|_{y'}^{y}\right\} . \tag{17}$$

where

z' = some arbitrary height

$$x = \left(1 - \beta\frac{z}{L}\right)^{1/4} \tag{18}$$

$$y = \left(1 - \gamma\frac{z}{L}\right)^{1/2} \tag{19}$$

$$y_L = \left(1 - \gamma\frac{z}{L_v}\right)^{1/2} . \tag{20}$$

Figure 3 illustrates a wind profile, as formulated in equation (15). Figure 3 shows that this curve is a realization of a strictly increasing monotonic functional form. If we properly select three points on this curve, that is, $z_1 < z_r < z_2$, we can apply the mean value theorem of calculus (see appendix A). Given a pair of points z_1 and z_2 the mean value theorem asserts there is a point z_r, $z_1 < z_r < z_2$ such that the chord connecting these points is parallel to the tangent line at z_r. Figure 3 also shows this relationship.

From equation (12) the derivative at z_r is

$$\left.\frac{\partial V}{\partial z}\right|_r = \frac{u^*}{k z_r}\left(1 + \beta \frac{z_r}{L}\right)^{1/4} \quad . \tag{21}$$

From the mean value theorem we can write

$$\frac{V(z_2)}{z_2} - \frac{V(z_1)}{z_1} = \left.\frac{\partial V}{\partial z}\right|_r \quad . \tag{22}$$

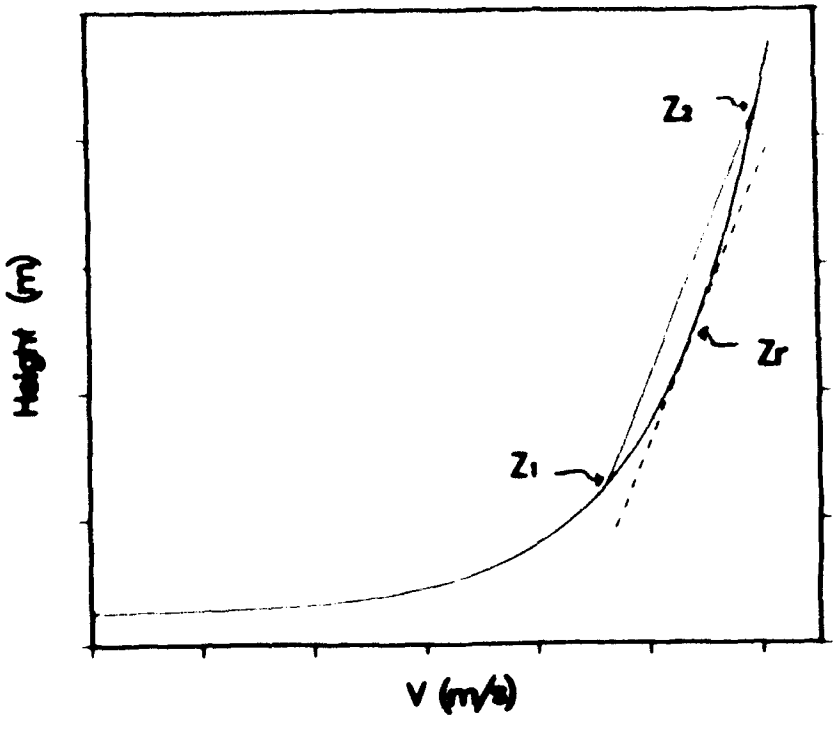

Figure 3. Illustrative wind profile as formulated in equation (15).

From equation (15) we can write

$$V(z_2) \quad V(z_1) = \frac{u^*}{k} \left\{ \ln\left(\frac{x}{x+1}\right) + 2\tan^{-1} x \right\}\Bigg|_{z_1}^{z_2} \quad . \tag{23}$$

Combining equations (21), (22), and (23) we obtain

$$\left\{ \ln\left(\frac{x}{x+1}\right) + 2\tan^{-1} x \right\}\Bigg|_{z_1}^{z_2} = \frac{(z_2 - z_1)}{z_{rv}} \left(1 - \beta \frac{z_r}{L}\right)^{-1/4} \quad . \tag{24}$$

Using equation (24) we can solve for z_{rv} for specified values of z_1 and z_2 and an estimate (first approximation) of L.

Using #, we can write an equation similar to equation (24) to solve for $z_{r\theta}$, that is,

$$\ln\left(\frac{y}{y+1}\right)\Bigg|_{z_1}^{z_2} = \frac{(z_2 - z_1)}{z_{r\theta}} \left(1 - \gamma \frac{z_{r\theta}}{L}\right)^{1/2} \quad . \tag{25}$$

Now we make use of measured data, and, as suggested in section 2, we draw a smooth curve through these measured data points. Having determined z_r for specified heights z_1 and z_2, we can evaluate $\left.\frac{\partial V}{\partial z}\right|_r$ using equation (20). Substituting this value into equation (21), we compute u^*, that is,

$$u^* = kz_r \frac{V(z_2) - V(z_1)}{z_2 - z_1} \left(1 - \beta \frac{z_r}{L}\right)^{1/4} \quad . \tag{26a}$$

In a similar fashion we compute T^*,

$$T^* = kz_{r\theta} \frac{T(z_2) - T(z_1)}{z_2 - z_1} \left(1 - \gamma \frac{z_{r\theta}}{L}\right)^{1/2} \tag{26b}$$

Note that for moderately unstable conditions $\frac{\partial \theta}{\partial z} = \frac{\partial T}{\partial z}$. Having computed u^* and θ^* for a first approximation for L, we then compute a second approximation for L using

$$L = \frac{u^{*2} T_r}{kg\theta^*} \quad . \tag{27}$$

The procedure for computing u^* and θ^* outlined above is repeated using the L values from equation (27) giving a second approximation for u^* and θ^*, which are then used to obtain a third approximation for L. This process is continued until u^*, θ^*, and L converge.

Having values for u^*, θ^*, and L, we then approximate q^* making use of equations (14) and (17).

Note, however, that equations (14) and (17) require L_v instead of L. We move in the direction of L_v by evaluating

$$L_v = \frac{u^{*2} T_{vr}}{kg\theta_v^*} \quad , \tag{28}$$

where

$$\theta_v^* = \theta^* + 0.61\, \theta_r\, q^* \quad . \tag{29}$$

Hence, even though the first approximation for q^* is based on L, the second approximation is based on L_v. This process is continued until q^* and L_v converge.

The overall procedure above is repeated for several pairs of values of z_1, z_2 giving sets of estimates of u^*, θ^*, q^*, L, and L_v. Each set of these values is averaged giving $\bar{u}^*$, $\bar{\theta}^*$, $\bar{q}^*$, $\bar{L}$, and $\bar{L}_v$. These average values are then used in equations (15) through (17) to compute vertical profiles of v, θ, and q.

An approach that we have used successfully for refining these values is to generate profile values using the average values of u^*, θ^*, q^*, L, and L_v. These values are then averaged with the original smoothed data values, and these averaged values are used in the solution procedure. This process is repeated until profile convergence is attained. This process assures that the final profiles are of the similarity form. This refinement is not considered in the study.

4. CALCULATION PROCEDURES

The traditional method presented in section 2 presumes that either measurements of wind and temperature or smoothed values are available at heights defined by a geometric series. As such, the basic data points represent discrete vertical profiles.

The first step in this computational procedure produces a discrete vertical potential temperature profile from the temperature values using the relationship

$$\theta = T + \Gamma z \quad , \tag{30}$$

where Γ is the dry adiabatic lapse rate.

The second step produces Richardson numbers for the geometric mean heights, that is, $z_g = (z_i\ z_{i-1})^{1/2}$, of pairs of heights z_i and z_{i-1}, using the expression

$$Ri = \frac{g}{T} \frac{(\theta_i - \theta_{i-1})}{(V_i - V_{i-1})^2} z_g \ln \frac{z_i}{z_{i-1}} \quad . \tag{31}$$

The third step makes use of the results of the second step to obtain estimates of the Obukhov length by using

$$L = \frac{z_g}{R_i} \quad . \tag{32}$$

Note equation (30) requires that $\beta = \gamma$.

The fourth step yields estimates of u^* and T^* using the relationships

$$u^* = \frac{(V_i - V_{i-1})\left[1 - 15 \frac{z_g}{L}\right]^{1/4}}{\ln \frac{z_i}{z_{i-1}}} \tag{33}$$

$$T^* = \frac{(\theta_i - \theta_{i-1})\left[1 - 15 \frac{z_g}{L}\right]^{-1/2}}{\ln \frac{z_i}{z_{i-1}}} \quad . \tag{34}$$

In the fifth step one computes average values of L, u*, and T* for the total layer of interest, $H = \sum_{i=1}^{n} (z_i - z_{i-1})$.

The RT procedure also presumes that temperature and wind data (measured or smoothed) are available at discrete heights, but not necessarily as defined by a geometric series.

The first and second steps in the RT procedure are the same as in the traditional procedure, that is, we use equation (30) to compute θ_i, knowing T_i and equation (31) to compute Ri.

The third step is used to compute L knowing R_i using the relationship

$$L^3 - \gamma z L^2 - \frac{z^2}{R_i^2} L + \frac{\beta z^3}{R_i^2} = 0 \qquad (35)$$

instead of equation (32). For $\gamma = \beta$ equation (33) reduces to equation (32), however.

The fourth step yields heights z_{rv} and $z_{r\theta}$, the heights between pairs of v_i, and pairs of θ that satisfy the mean value theorem constraints. The expressions that satisfy these constraints are given by equations (24) and (25). Unfortunately, these expressions must be solved for z_{rv} and $z_{r\theta}$ by iteration. We use z_g as a first approximation for z_{rv} and $z_{r\theta}$.

The fifth step produces estimates of u* and T* using equations (26a) and (26b).

In the sixth step u* and T* of step 5 are used in equation (27) to compute a new estimate of L if necessary, and the above process is repeated until u*, T*, and L converge.

5. RESULTS

To clearly illustrate the differences between our method of determining $z_r(v)$ and $z_r(\theta)$ and the profile smoothing technique, which assumes z_r to be equal to the geometric mean of z_1 and z_2, we have chosen two purely theoretical case studies. The first case considers the neutral atmosphere. The second case focuses on an atmosphere that is characterized as strongly unstable. For each case we assign a roughness length (z_o) of 1 cm, a reference height temperature of 30 °C, and select z_1 and z_2 equal to 1 and 4 m, respectively. In addition, both β and γ are set equal to 15. The similarity scaling and Obukhov lengths chosen are shown in table 2 as well as our computed reference

heights. Note the numbers in parentheses reflect those constants computed by the traditional method. They are clearly equivalent to those of the RT method.

In figure 4 we present the windspeed profile derived from the two methods discussed in this report for the neutral case. Figures 5 and 6 depict the wind and temperature profiles, respectively, for the unstable case. Note that the two methods give equivalent representation of the wind and temperature structure in the lower boundary layer.

TABLE 2. SIMILARITY CONSTANTS AND COMPUTED REFERENCE HEIGHTS

Neutral Case	$u^* = 0.4$ m/s	$z_r(v) = 2.16$ m
	$T^* = 0.0$	
	$L = \infty$	
Unstable Case	$u^* = 0.4$ m/s	$z_r(v) = 2.15$ m
	($u^* = 0.398$ m/s)	$z_r(\theta) = 2.13$ m
	$T^* = -0.5$ °C	
	($T^* = -0.498$ °C)	
	$L = -24.74$ m	
	($L = -24.67$ m)	

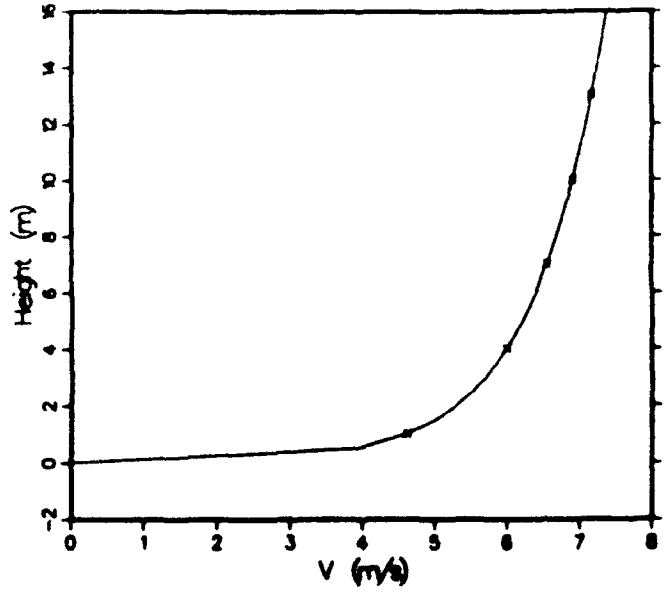

Figure 4. Windspeed profile in the surface boundary layer for the neutral case. (x's trace the traditional approach.)

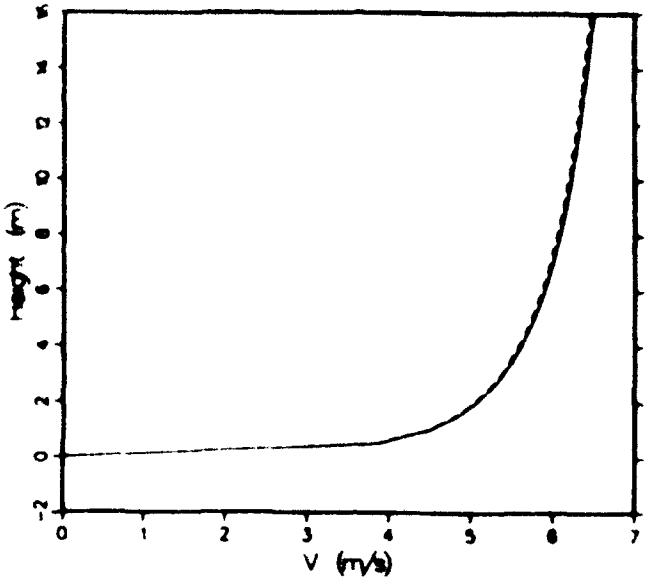

Figure 5. Windspeed profiles in the surface boundary layer for the unstable case. Traditional approach (dashed line).

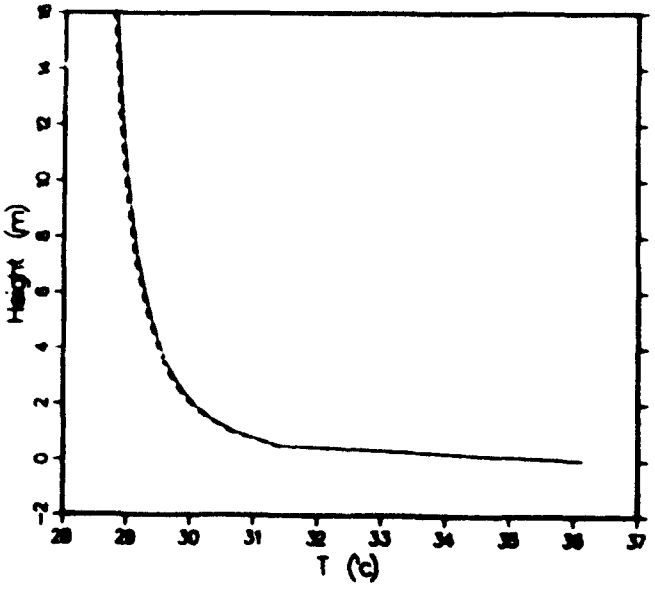

Figure 6. Temperature profiles in the surface boundary layer for the unstable case. Traditional approach (dashed line).

6. CONCLUSIONS

Note that the exacting mean value theorem of calculus can be excellently approximated by the application of a lognormal, geometric progression. The differences in the derived values of u^*, T^*, L, $\bar{V}$, and $\bar{\theta}$ from both approaches are not significant. This mean value theorem may be interpreted geometrically, for it states that a tangent to a smooth curve is parallel to any intermediate point on a chord of the curve. Generalization leads to an extended* mean value theorem.

No formal documentation of the melding of geometric progressions and the extended mean value theorem has been discovered; however, we did find that the law of natural increase had some solid footing in mathematics.

Results from the two examples considered in this report show that the differences in u^*, T^*, L, V, and θ using the traditional and RT modules are not significant. Furthermore, there is less labor required in executing the traditional model than the RT model. This aspect may have been the motivation for the design of the traditional approach.

However, if $\beta \neq \gamma$, then the relationship $R_i = z/L$ should be replaced by equation (35) in the traditional approach.

Finally, it was gratifying to find that this problem lent itself to such a good and reasonable solution by using the mean value theorem.

*Van Nostrand's Scientific Encyclopedia, Seventh edition, D. M. Considine, ed., Van Nostrand Reinhold, New York

LITERATURE CITED

Businger, J. A., J. C. Wyngaard, Y. Izumi, and E. F. Bradley, 1971, "Flux-Profile Relationships in the Atmospheric Surface Layer," J Atmos Sci, 28:181-189.

Ellison, T. H., 1957, "Turbulent Transport of Heat Momentum from an Infinite Rough Plane," J Fluid Mech, 2:456-466.

Hansen, F. V., 1977, The Critical Richardson Number, ECOM-5829, U.S. Army Atmospheric Sciences Laboratory, White Sands Missile Range, NM 88002-5501.

Hicks, B. B., 1976, "Wind Profile Relationships from the Wangara Experiment," Quart J Roy Meteorol Soc, 102:535-551.

Lettau, H. H., 1957, "Computation of Richardson Numbers, Classification of Wind Profiles, and Determination of Roughness Parameters," Exploring the Atmosphere's First Mile, Vol. 1, (H. H. Lettau and B. Davidson, eds), Pergamon Press, New York.

Monin, A. S., and Obukhov, A. M., 1954, "Basic Regularity in Turbulent Mixing in the Surface Layer of the Atmosphere," Trans Geophys Inst (Trudy) Acad Sci, USSR, 24:163-187.

Obukhov, A. M., 1946, "Turbulence in an Atmosphere of Non-Homogeneous Temperature," Trans Inst Theor Geophy, USSR, 1:95-115.

Oke, T. K., 1970, "Turbulent Transport Near the Ground in Stable Conditions," J Appl Meteorol Soc, 9:778-786.

Panofsky, H. A., 1963, "Determination of Stress from Wind and Temperature Measurements," Quart J Roy Meteorol Soc, 89:85-94.

Richardson, L. F., 1920, "The Supply of Energy from and to Atmospheric Eddies," Proc Roy Soc, A, 97:354-373.

Sutherland, R. A., F. V. Hansen, and W. D. Bach, 1986, "A Quantitative Method for Estimating Pasquill Stability Class from Windspeed and Sensible Heat Flux Density," Boundary Layer Meteorology, 37:357-369.

Sutton, O. G., 1953, Micrometeorology, McGraw and Hill Book Company, Incorporated, New York, Toronto, London.

Webb, E. K., 1970, "Profile Relationships: The Log-Linear Range and Extension to Strong Stability," Quart J Roy Meteorol Soc, 96:67-90.

APPENDIX A. RACHELE/TURICK (RT) APPROACH

Neutral Case

Let

$$\frac{\partial V}{\partial z} = \frac{V^*}{kz} \tag{A-1}$$

then

$$V = \frac{V^*}{k} \ln\left(\frac{z}{z_o}\right) \tag{A-2}$$

From equation (A-2)

$$V_2 \quad V_1 = \frac{V^*}{k} \ln\left(\frac{z_2}{z_1}\right) \tag{A-3}$$

Dividing equation (A-3) by $(z_2 \quad z_1)$ gives

$$\frac{V_2}{z_2} \quad \frac{V_1}{z_1} = \frac{V^*}{k(z_2 - z_1)} \ln\left(\frac{z_2}{z_1}\right) \tag{A-4}$$

From the mean value theorem

$$\frac{V_2}{z_2} \quad \frac{V_1}{z_1} = \left.\frac{\partial V}{\partial z}\right|_{z_r} \quad \text{where } z_1 < z_r < z_2 \tag{A-5}$$

From equations (A-1), (A-4), and (A-5)

$$\frac{V_2 - V_1}{z_2 - z_1} = \left.\frac{\partial V}{\partial z}\right|_{z_r} = \frac{V^*}{kz_r} = \frac{V^*}{k(z_2 - z_1)} \ln\left(\frac{z_2}{z_1}\right) \tag{A-6}$$

Solving equation (A-6) for z_r gives

$$z_r = \frac{(z_2 - z_1)}{\ln\left(\frac{z_2}{z_1}\right)} \qquad \text{(A-7)}$$

Now suppose that z_1 = 100 cm and z_2 = 400 cm,

then z_r = 216.40425 cm.

Now consider the case where V^* = 20 cm/s and z_o = 1 cm, then

$$V(400) = 299.57322$$

$$V(100) = 230.25850$$

From equation (A-5)

$$\left.\frac{\partial V}{\partial z}\right|_{zr} = 0.231049$$

Assuming z_r = 200 cm, and using equation (A-6), we get

$$V^* = \left.\frac{\partial V}{\partial z}\right|_{z_r} kz_r = 0.231049(.4)(200)$$

$$= 18.484$$

So : V(100) = 212.805

$$\left.\frac{\partial V}{\partial z}\right|_{z_r} = 0.23536$$

Unstable Case

$$\frac{V_2}{z_2} - \frac{V_2}{z_1} = \frac{V^*}{kz_r}\left(1 - 15\,\frac{z_r}{L}\right)^{1/4} \tag{A-8}$$

$$\frac{T_2}{z_2} - \frac{T_1}{z_1} = \frac{T^*}{kz_r}\left(1 - 15\,\frac{z_r}{L}\right)^{1/2} \tag{A-9}$$

$$L = \frac{V^{*2}T_r}{kg\,T^*} \tag{A-10}$$

$$z_r(v) = \left(z_2 - z_1\right)\left(1 - 15\,\frac{z_r}{L}\right)^{1/4} \Bigg/ \ln\left(\frac{x-1}{x+1}\right)\Bigg|_{z_1}^{z_2} \tag{A-11}$$

$$z_r(\theta) = \left(z_2 - z_1\right)\left(1 - 15\,\frac{z_r}{L}\right)^{1/2} \Bigg/ \ln\left(\frac{y-1}{y+1}\right)\Bigg|_{y_1}^{y_2} \tag{A-12}$$

where

$$x = \left(1 - 15\,\frac{z}{L}\right)^{1/4}, \quad y = \left(1 - 15\,\frac{z}{L}\right)^{1/2} \tag{A-13}$$

Stable Case

Let

$$\frac{\partial V}{\partial z} = \frac{V^*}{kz}\left(1 + 5\,\frac{z}{L}\right) \tag{A-14}$$

then

$$V = \frac{V^*}{k}\left(\ln\frac{z}{z_o} + 5\,\frac{z}{L}\right) \tag{A-15}$$

From equation (A-15)

$$V_2 - V_1 = \frac{V^*}{k}\left[\ln\frac{z_2}{z_1} + 5\frac{(z_2 - z_1)}{L}\right] \qquad \text{(A-16)}$$

Dividing equation (A-16) by $(z_2 - z_1)$ gives

$$\frac{V_2 - V_1}{z_2 - z_1} = \frac{V^*}{k(z_2 - z_1)}\left[\ln\frac{z_2}{z_1} + 5\frac{(z_2 - z_1)}{L}\right] \qquad \text{(A-17)}$$

From the mean value theorem

$$\frac{V_2 - V_1}{z_2 - z_1} = \left.\frac{\partial V}{\partial z}\right|_r \quad \text{where } z_1 < z_r < z_2 \qquad \text{(A-18)}$$

From equations (A-14), (A-17), and (A-18)

$$\frac{V_2 - V_1}{z_2 - z_1} = \left.\frac{\partial V}{\partial z}\right|_{z_r} = \frac{V^*}{kz_z}\left[1 + 5\frac{z_r}{L}\right] = \frac{V^*}{k(z_2 - z_1)}\left[\ln\frac{z_2}{z_1} + 5\frac{(z_2 - z_1)}{L}\right] \qquad \text{(A-19)}$$

Solving equation (A-19) implicitly for z_r gives

$$z_r = \frac{(z_2 - z_1)\left[1 + 5\frac{z_r}{L}\right]}{\left[\ln\frac{z_2}{z_1} + 5\frac{(z_2 - z_1)}{L}\right]} \qquad \text{(A-20)}$$

APPENDIX B. THEOREM OF THE MEAN

If $f(x)$ is continuous in the interval $a \leq x \leq b$ and has a derivative between $x = a$ and $x = b$, then

$$f(b) - f(a) = (b - a)f'(\xi) \tag{B-1}$$

where

$$a < \xi < b.$$

Equation (B-1) is illustrated in the figure below

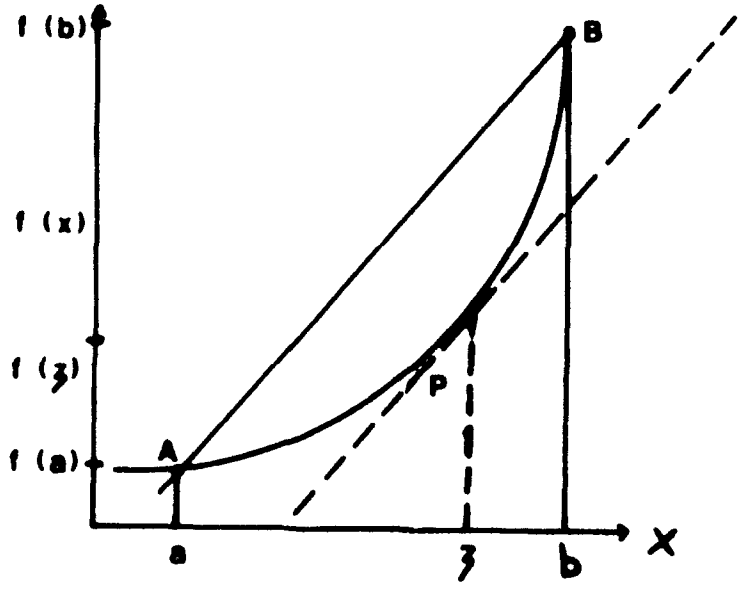

Figure B-1. Illustration of the mean value theorem for a given function $f(x)$.

The theorem asserts that there is a point (p) at which the tangent $f'(\xi)$ is parallel to the chord AB.

If we let $f(x) = V(z)$, then equation (B-1) can be written as

$$\left.\frac{dV}{dz}\right|_{\xi} = \frac{V(b) - V(a)}{z_b - z_a} \tag{B-2}$$

DISTRIBUTION LIST FOR PUBLIC RELEASE

Commandant
U.S. Army Chemical School
ATTN: ATZN-CM-CC (S. Barnes)
Fort McClellan, AL 36205-5020

Commander
U.S. Army Aviation Center
ATTN: ATZQ-D-MA
Mr. Oliver N. Heath
Fort Rucker, AL 36362

Commander
U.S. Army Aviation Center
ATTN: ATZQ-D-MS (Mr. Donald Wagner)
Fort Rucker, AL 36362

NASA/Marshall Space Flight Center
Deputy Director
Space Science Laboratory
Atmospheric Sciences Division
ATTN: E501 (Dr. George H. Fichtl)
Huntsville, AL 35802

NASA/Marshall Space Flight Center
Atmospheric Sciences Division
ATTN: Code ED-41
Huntsville, AL 35812

Deputy Commander
U.S. Army Strategic Defense Command
ATTN: CSSD-SL-L
Dr. Julius Q. Lilly
P.O. Box 1500
Huntsville, AL 35807-3801

Commander
U.S. Army Missile Command
ATTN: AMSMI-RD-AC-AD
Donald R. Peterson
Redstone Arsenal, AL 35898-5242

Commander
U.S. Army Missile Command
ATTN: AMSMI-RD-AS-SS
Huey F. Anderson
Redstone Arsenal, AL 35898-5253

Commander
U.S. Army Missile Command
ATTN: AMSMI-RD-AS-SS
B. Williams
Redstone Arsenal, AL 35898-5253

Commander
U.S. Army Missile Command
ATTN: AMSMI-RD-DE-SE
Gordon Lill, Jr.
Redstone Arsenal, AL 35898-5245

Commander
U.S. Army Missile Command
Redstone Scientific Information
Center
ATTN: AMSMI-RD-CS-R/Documents
Redstone, Arsenal, AL 35898-5253

Commander
U.S. Army Intelligence Center
and Fort Huachuca
ATTN: ATSI-CDC-C (Mr. Colanto)
Fort Huachuca, AZ 85613-7000

Northrup Corporation
Electronics Systems Division
ATTN: Dr. Richard D. Tooley
3301 West 120th Street, Box 5032
Hawthorne, CA 90251-5032

Commander - Code 3331
Naval Weapons Center
ATTN: Dr. Alexis Shlanta
China Lake, CA 93555

Commander
Pacific Missile Test Center
Geophysics Division
ATTN: Code 3250-3 (R. de Violini)
Point Mugu, CA 93042-5000

Commander
Pacific Missile Test Center
Geophysics Division
ATTN: Code 3250 (Terry E. Battalino)
Point Mugu, CA 93042-5000

Lockheed Missiles & Space Co., Inc.
Kenneth R. Hardy
Org/91-01 B/255
3251 Hanover Street
Palo Alto, CA 94304

Commander
Naval Ocean Systems Center
ATTN: Code 54 (Dr. Juergen Richter)
San Diego, CA 92152-5000

Meteorologist in Charge
Kwajalein Missile Range
P.O. Box 67
APO San Francisco, CA 96555

U.S. Department of Commerce
Mountain Administration Support
Center
Library, R-51 Technical Reports
325 S. Broadway
Boulder, CO 80303

Dr. Hans J. Liebe
NTIA/ITS S 3
325 S. Broadway
Boulder, CO 80303

NCAR Library Serials
National Center for Atmos Rsch
P.O. Box 3000
Boulder, CO 80307-3000

Bureau of Reclamation
ATTN: D: 1200
P.O. Box 25007
Denver, CO 80225

HQDA
ODCSOPS
ATTN: DAMO-FDZ
Washinting, D.C. 20310-0460

Mil Asst for Env Sci Ofc of
The Undersecretary of Defense
for Rsch & Engr/R&AT/E&LS
Pentagon - Room 3D129
Washington, D.C. 20301-3080

Director
Naval Research Laboratory
ATTN: Code 4110
Dr. Lothar H. Ruhnke
Washington, D.C. 20375-5000

HQDA
DEAN-RMD/Dr. Gomez
Washington, D.C. 20314

Director
Division of Atmospheric Science
National Science Foundation
ATTN: Dr. Eugene W. Bierly
1800 G. Street, N.W.
Washington, D.C. 20550

Commander
Space & Naval Warfare System Command
ATTN: PMW-145-1G (LT Painter)
Washington, D.C. 20362-5100

Commandant
U.S. Army Infantry
ATTN: ATSH-CD-CS-OR
Dr. E. Dutoit
Fort Benning, GA 30905-5090

USAFETAC/DNE
Scott AFB, IL 62225

Air Weather Service
Technical Library - FL4414
Scott AFB, IL 62225-5458

HQAWS/DOZ
Scott AFB, IL 62225-5008

USAFETAC/DNE
ATTN: Mr. Charles Glauber
Scott AFB, IL 62225-5008

Commander
U.S. Army Combined Arms Combat
ATTN: ATZL-CAW (LTC A. Kyle)
Fort Leavenworth, KS 66027-5300

Commander
U.S. Army Combined Arms Combat
ATTN: ATZL-CDB-A (Mr. Annett)
Fort Leavenworth, KS 66027-5300

Commander
U.S. Army Space Institute
ATTN ATZI-SI (Maj Koepsell)
Fort Leavenworth, KS 66027-5300

Commander
U.S. Army Space Institute
ATTN ATZL-SI-D
Fort Leavenworth, KS 66027-7300

OL AA PL/LYP
ATTN: Mr. Chisholm
Hanscom AFB, MA 01731-5000

OL AA PL/LY
ATTN: Dr. Robert A. McClatchey
Hanscom AFB, MA 01731-5000

Raytheon Company
Dr. Charles M. Sonnenschein
Equipment Division
528 Boston Post Road
Sudbury, MA 01776
Mail Stop 1K9

Director
U.S. Army Materiel Systems
Analysis Activity
ATTN: AMXSY-MP (H. Cohen)
APG, MD 21005-5071

Commander
U.S. Army Chemical Rsch,
Dev & Engr Center
ATTN: SMCCR-OPA (Ronald Pennsyle)
APG, MD 21010-5423

Commander
U.S. Army Chemical Rsch,
Dev & Engr Center
ATTN: SMCCR-TDT (Mr. Joseph Vervier)
APG, MD 21010-5423

Commander
U.S. Army Chemical Rsch,
Dev & Engr Center
ATTN: SMCCR-MUC (Mr. A. Van De Wal)
APG, MD 21010-5423

Director
U.S. Army Materiel Systems
Analysis Activity
ATTN: AMXSY-GC (Mr. Fred Campbell)
APG, MD 21005-5071

Director
U.S. Army Materiel Systems
Analysis Activity
ATTN: AMXSY-CR (Robert N. Matchett)
APG, MD 21005-5071

Director
U.S. Army Materiel Systems
Analysis Activity
ATTN: AMXSY-CS (Mr. Brad W. Bradley)
APG, MD 21005-5071

Commander
U.S. Army Laboratory Command
ATTN: AMSLC-CG
2800 Powder Mill Road
Adelphi, MD 20783-1145

Commander
Headquarters
U.S. Army Laboratory Command
ATTN: AMSLC-CT
2800 Powder Mill Road
Adelphi, MD 20783-1145

Commander
Harry Diamond Laboratories
ATTN: SLCIS-CO
2800 Powder Mill Road
Adelphi, MD 20783-1197

Director
Harry Diamond Laboratories
ATTN: SLCHD-RT-AC
Dr. Z.G. Sztankay
Adelphi, MD 20783-1197

Air Force Systems Command/WER
Andrews AFB, MD 20334-5000

National Security Agency
ATTN: W21 (Dr. Longbothum)
9800 Savage Road
Ft George G. Meade, MD 20755-6000

Officer in Charge
Naval Surface Weapons Center
White Oak Library
Technical Library
Silver Springs, MD 20910-1090

The Environmental Research
Institute of MI
ATTN: IRIA Library
P.O. Box 8618
Ann Arbor, MI 48107-8618

Commander
U.S. Army Research Office
ATTN: DRXRO-GS (Dr. W.A. Flood)
P.O. Box 12211
Research Triangle Park, NC 27709

Dr. Jerry Davis
North Carolina State University
Department of Marine, Earth, &
Atmospheric Sciences
P.O. Box 8208
Raleigh, NC 27650-8208

Commander
U.S. Army Cold Regions Research
& Engineering Laboratory
ATTN: CRREL-RG (Mr. Robert Redfield)
Hanover, NH 03755-1290

Commander
U.S. Army Cold Regions Research
& Engineering Laboratory
ATTN: CECRL-RD (Dr. K.F. Sterrett)
Hanover, NH 03755-1290

Commanding Officer
U.S. Army Armament R&D Command
ATTN: DRDAR-TSS, Bldg 59
Dover, NJ 07801

U.S. Army Communications-Electronics
Command Center for EW/RSTA
ATTN: AMSEL-RD-EW-SP
Fort Monmouth, NJ 07703-5303

Commander
U.S. Army Communications-Electronics
Command
ATTN: AMSEL-EW-D (File Copy)
Fort Monmouth, NJ 07703-5303

Headquarters
U.S. Army Communications Electronics
Command
ATTN: AMSEL-EW-MD
Fort Monmouth, NJ 07703-5303

Commander
U.S. Army Satellite Comm Agency
ATTN: DRCPM-SC-3
Fort Monmouth, NJ 07703-5303

Director
EW/RSTA Center
ATTN: AMSEL-EW-DR
Fort Monmouth, NJ 07703-5303

USACECOM
Center for EW/RSTA
ATTN: AMSEL-RD-EW-SP
Fort Monmouth, NJ 07703-5303

6585th TG (AFSC)
ATTN: RX (CPT Stein)
Holloman AFB, NM 88330

Department of the Air Force
OL/A 2nd Weather Squadron (MAC)
Holloman AFB, NM 88330-5000

PL/WE
Kirtland AFB, NM 87118-6008

Director
U.S. Army TRADOC Analysis Command
ATTN: ATRC-WSS-R
White Sands Missile Range, NM 88002

Rome Laboratory
ATTN: Technical Library RL/DOVL
Griffiss AFB, NY 13441-5700

Department of the Air Force
7th Squadron
APO, NY 09403

AWS
USAREUR/AEAWX
APO, NY 09403-5000

AF Wright Aeronautical Laboratories
Avionics Laboratory
ATTN: AFWAL/AARI (Dr. V. Chimelis)
Wright-Patterson AFB, OH 45433

Commander
U.S. Army Field Artillery School
ATTN: ATSF-F-FD (Mr. Gullion)
Fort Sill, OK 73503-5600

Commandant
U.S. Army Field Artillery School
ATTN: ATSF-TSM-TA
Mr. Charles Taylor
Fort Sill, OK 73503-5600

Commander
Naval Air Development Center
ATTN: Al Salik (Code 5012)
Warminster, PA 18974

Commander
U.S. Army Dugway Proving Ground
ATTN: STEDP-MT-DA-M
Mr. Paul Carlson
Dugway, UT 84022

Commander
U.S. Army Dugway Proving Ground
ATTN: STEDP-MT-DA-L
Dugway, UT 84022

Commander
U.S. Army Dugway Proving Ground
ATTN: STEDP-MT-M (Mr. Bowers)
Dugway, UT 84022-5000

Defense Technical Information Center
ATTN: DTIC-FDAC
Cameron Station
Alexandria, VA 22314

Commanding Officer
U.S. Army Foreign Science &
Technology Center
ATTN: CM
220 7th Street, NE
Charlottesville, VA 22901-5396

Naval Surface Weapons Center
Code G63
Dahlgren, VA 22448-5000

Commander
U.S. Army OEC
ATTN: CSTE-EFS
Park Center IV
4501 Ford Ave
Alexandria, VA 22302-1458

Commander and Director
U.S. Army Corps of Engineers
Engineer Topographics Laboratory
ATTN: ETL-GS-LB
Fort Belvoir, VA 22060

Department of the Air Force
HQ 5 Weather Wing (MAC)
ATTN: 5 WW/DN
Langley AFB, VA 23665-5000

Commander and Director
U.S. Army Corps of Engineers
Engineer Topographics Laboratory
ATTN: CEETL-ZD
Fort Belvoir, VA 22060-5546

Commander
Logistics Center
ATTN: ATCL-CE
Fort Lee, VA 23801-6000

Commander
USATRADOC
ATTN: ATCD-FA
Fort Monroe, VA 23651-5170

Science and Technology
101 Research Drive
Hampton, VA 23666-1340

Commander
U.S. Army Nuclear & Cml Agency
ATTN: MONA-ZB Bldg 2073
Springfield, VA 22150-3198